Single-nucleon transfer to unbound states by means of the ^{4}He(α,^{3}He)^{5}He reaction at 158 and 200 MeV

G. F. Steyn, S. V. Förtsch, J. J. Lawrie, F. D. Smit, and R. T. Newman
National Accelerator Centre, Faure, 7131, South Africa

A. A. Cowley
Department of Physics, University of Stellenbosch, Stellenbosch, 7600, South Africa

R. Lindsay
Department of Physics, University of the Western Cape, Bellville, 7535, South Africa
(Received 9 May 1996)

The ^{4}He(α,^{3}He)^{5}He(g.s.) reaction was studied at incident laboratory energies of 158 and 200 MeV for c.m. scattering angles ranging from $\sim$16° to 100°. The shape of the ^{5}He(g.s.) peak in the measured ^{3}He energy spectra is well reproduced by distorted-wave Born approximation calculations. Whereas calculations utilizing six-parameter optical potentials yield good qualitative agreement with the measured angular distributions, unacceptably poor agreement is found when nine-parameter potentials are utilized. Absolute normalization with D_0^2 strengths extracted from corresponding zero-range and finite-range calculations overpredicts the measurements by factors of $\sim$2 to 3. [S0556-2813(96)06210-3]

PACS number(s): 24.10.Eq, 25.55.Hp, 27.10.+h

I. INTRODUCTION

Recently, the distorted-wave Born approximation (DWBA) was employed with reasonable success in predicting the angular distribution of the ^{4}He(α,^{3}He)^{5}He(g.s.) reaction at 118 MeV [1]. Also, when effects leading to the broadening of the ^{5}He(g.s.) peak were taken into account, excellent agreement in shape was found between calculations and the relevant regions in the measured ^{3}He energy spectra corresponding to $0 \leqslant \epsilon \leqslant 5$ MeV, where ϵ is the relative α-n energy in the ^{5}He system. The above-mentioned peak is due to single-nucleon transfer to a resonant neutron state in ^{5}He with a width of $\Gamma = 0.60$ MeV, for which $\epsilon = 0.89$ MeV [2]. The absolute magnitude of the cross sections, however, is overpredicted by a factor of $\sim$2 at 118 MeV.

The DWBA is generally considered to be more reliable when the bombarding energy is high compared to the binding energy of the transferred nucleon [3]. Since the transferred neutron is bound by 20.58 MeV in ^{4}He, an investigation at higher incident energies should be useful to explore the findings and conclusions of the 118 MeV experiment further. Our present work is such an investigation at 158 and 200 MeV.

Elastic scattering differential cross sections for the reaction ^{4}He(α,α)^{4}He were measured at the same time for comparison with existing data and in order to extract optical-model parameters needed for the DWBA calculations. While a single set of consistent elastic scattering data existed at 158 MeV [4], the two available data sets at 200 MeV [5,6] appear to differ by more than the expected uncertainty. Consequently, the discrepancies in the existing 200 MeV data precluded optical-model fits of sufficient accuracy for the extraction of reliable optical-model parameters. Values extracted for six- as well as nine-parameter optical-model potentials [4] from the new elastic scattering data, using Woods-Saxon wells, are therefore also presented in this study. The energy dependence of the real and imaginary volume integrals was also investigated to provide guidance in assessing the accuracy of the new elastic scattering data.

In Sec. II the experimental setup is described, followed by a description in Sec. III of the data analysis. The details of the DWBA calculations are described in Sec. IV. In Sec. V the experimental and theoretical results are compared and discussed. Finally, a summary and conclusions are presented in Sec. VI.

II. EXPERIMENTAL PROCEDURE

The experiment was performed by utilizing the 1.5-m-diameter scattering chamber at the cyclotron facility of the National Accelerator Centre, Faure. An account of the facility has been presented in Ref. [7] and references therein.

A 100-mm-diameter gas cell, filled with helium ($>$99.995% purity) to a nominal absolute pressure of 1.5 bar at room temperature, was bombarded with α particles of 158.5 and 200.5 MeV, respectively. The uncertainty in the quoted beam energies is not greater than 0.5 MeV. The pressure and temperature of the target gas were monitored continuously by means of calibrated transmitters, to a precision of better than 1%. The beam-spot size was less than 3 mm in diameter and remained centered on target to better than 0.5 mm. The scattering angle was determined to better than 0.05°.

The effective target length and solid angle were defined by means of a double-aperture collimator system with 3 mm thick tantalum front and rear slits. The slits were placed 186 and 526 mm, respectively, from the center of the target. The rather large distance from the gas cell and large separation between slits ensured that measurements could be performed down to very forward angles (8° in the laboratory system)

with small effective target lengths and good angular resolution, albeit at the cost of a reduction in count rate. Two sets of equal-width, rectangular front and rear slits were used. At forward angles smaller than 26° (laboratory), 2.8 mm wide slits were used, while 4.5 mm wide slits were employed at larger angles in order to increase the count rate. The 2.8 mm slits defined a solid angle of 0.12 msr and an angular resolution of 0.5°, while the corresponding values for the 4.5 mm slits are 0.2 msr and 0.8°, respectively. The effective target length varied between 8 and 28 mm, i.e., well distant from the 6 μm thick Havar entrance and exit windows of the gas cell.

Different detector telescopes were used in the 158 and 200 MeV measurements. For the 158 MeV runs the telescope consisted of a 150 μm thick Si surface-barrier ΔE detector, followed by two Si-Li detectors of 5 mm nominal thickness each, followed by a 1 mm thick Si surface-barrier veto detector. For the 200 MeV runs the front ΔE element was replaced with a 2 mm thick Si surface-barrier detector. Energy calibrations were based on collimated α particles from a ^{228}Th source as well as on the kinematics of ^{4}He(α,α)^{4}He elastic scattering. The standard ΔE-E technique was used for particle identification.

Conventional electronics were used to process signals from the detectors and event-by-event data were written to tape by the on-line computer for subsequent off-line analysis. Due to the rather small solid angles, count rates were generally low and dead times never exceeded the 1% level. Measurements were performed at 1° intervals, covering the laboratory angular region 8°–50°. Based on the various experimental uncertainties, the cross sections are estimated to be accurate to within a systematic error of 5%.

III. DATA ANALYSIS

Center-of-mass differential cross sections for the ^{4}He($\alpha,^3$He)^{5}He(g.s.) reaction were extracted from the measured ^{3}He energy spectra. This analysis consisted principally of two procedures. Firstly, the relevant part of each ^{3}He energy spectrum corresponding to $0 \leqslant \epsilon \leqslant 5$ MeV had to be determined in order to obtain the experimental ^{5}He(g.s.) yield (denoted by $Y_{\rm exp}$). Secondly, for each laboratory scattering angle, the mean α-n relative energy, $\langle\epsilon\rangle$, and the mean c.m. scattering angle, $\langle\theta\rangle$, had to be determined. Mean c.m.-to-laboratory conversion factors (relativistic Jacobians) $\langle J\rangle = J(\langle\epsilon\rangle,\langle\theta\rangle)$ could then also be obtained from kinematics.

In general, the yield Y and the c.m. double-differential cross section $\sigma(\epsilon,\theta)$ are related by [1]

$$Y = \nu N_0 \int_0^{t_{\rm max}} dt \int_\Omega d\Omega \int_0^{\epsilon^*} J(\epsilon,\theta)\sigma(\epsilon,\theta)d\epsilon, \qquad (1)$$

where ν is the number of incident particles, N_0 is the number of target nuclei per unit volume, and ϵ^* is an upper integration limit for the α-n relative energy, which was taken to be 5 MeV in accordance with Ref. [1]. The integration is over the total target length, t, the laboratory solid angle of the detection system, Ω, and the α-n relative energy, ϵ. The integrand consists of the Jacobian, J, and the double-differential cross section, σ, both of which are functions of ϵ and the c.m. scattering angle θ. The inverse solution for $\sigma(\epsilon,\theta)$ from Eq. (1) cannot be readily obtained, therefore some further simplifying assumptions have to be made.

First, we assumed that $\sigma(\epsilon,\theta)$ in the integrand of Eq. (1) is separable, i.e.

$$\sigma(\epsilon,\theta) = \phi(\theta)\sigma'(\epsilon). \qquad (2)$$

Next, we assumed that the shape of the angular distribution, $\phi(\theta)$, could be estimated sufficiently from the measured spectra and, if necessary, be refined iteratively as the analysis developed. If it could then be shown that DWBA calculations can reproduce the shapes of the ^{5}He(g.s.) peaks and therefore predict $\sigma'(\epsilon)$, calculated DWBA cross sections could be substituted into Eq. (1) to obtain $\langle\epsilon\rangle$ and $\langle\theta\rangle$. [The mean relative energy is found by multiplying the integrand in Eq. (1) by ϵ and by dividing the resulting integral by the original integral. The mean scattering angle is found similarly.] It should be noted that any good empirical fits to the relevant regions of the ^{3}He energy spectra could have been utilized for this purpose, but DWBA calculations were used in this case since they were required in the eventual interpretation of the measured angular distributions. Following Ref. [1], an energy-integrated differential cross section can be defined by

$$\sigma_{\epsilon^*}(\theta) = \int_0^{\epsilon^*} \sigma(\epsilon,\theta)d\epsilon. \qquad (3)$$

Equation (1) can then be simplified to

$$Y = \nu N_0 \langle J\rangle \sigma_{\epsilon^*}(\theta) \int_0^{t_{\rm max}} \int_\Omega dt d\Omega. \qquad (4)$$

The measured differential cross sections can therefore be obtained from

$$\sigma_{\epsilon^*}(\theta)_{\rm exp} = \frac{Y_{\rm exp}}{\nu N_0 \langle J\rangle \int_0^{t_{\rm max}} \int_\Omega dt d\Omega}. \qquad (5)$$

The values obtained for $\langle\epsilon\rangle$ mostly varied between 1.3 and 1.9 MeV with averages of 1.75 and 1.51 MeV at incident energies of 158 and 200 MeV, respectively. The mean α-n relative energies are therefore shifted from the values corresponding to the ^{5}He(g.s.)-peak maxima, which all lie at or close to $\epsilon = 0.89$ MeV. The differences between values calculated for $\langle\theta\rangle$ and the angles defined by the central rays were found to be insignificant, being only a few hundredths of a degree at all relevant angles.

A first set of experimental cross sections were obtained by using Jacobians calculated with $\epsilon = 0.89$ MeV for central rays, and by roughly estimating the lower integration limits for the ^{3}He energy in extracting values for $Y_{\rm exp}$. A new refined set of cross sections were then obtained after determining values for $\langle\epsilon\rangle$ and $\langle J\rangle$, fitting DWBA calculations to the measured ^{3}He spectra, and redetermining ^{3}He-energy integration limits corresponding to $\epsilon = 5$ MeV. In the same way one further iteration was performed, yielding no significant improvement to the previous values. Final cross-section values for the ^{4}He($\alpha,^3$He)^{5}He(g.s.) reaction were therefore obtained after two iterations.

TABLE I. Summary of optical-model parameters used in this study. The optical potential is defined as follows: $V_{\rm opt}=-V_1 f(r,r_1,a_1)-V_2 f(r,r_2,a_2)-iWf(r,r_w,a_w)+V_c$, where $f(r,r_i,a_i)=[1+\exp((r-r_iA^{1/3})/a_i)]^{-1}$; A is the target mass; V_c is the Coulomb potential of a uniform sphere of charge of radius[a] $r_cA^{1/3}$; and E_α is the incident laboratory kinetic energy.

E_α (MeV)	Pot. set	V_1 (MeV)	r_1 (fm)	a_1 (fm)	V_2 (MeV)	r_2 (fm)	a_2 (fm)	W (MeV)	r_w (fm)	a_w (fm)	Ref.
118	WAR118	48.55	1.792	0.596	64.50	0.632	0.243	8.580	2.202	0.287	[1]
158	NAD158a	53.75	1.628	0.613	43.97	0.545	0.142	9.623	2.094	0.467	[4]
	NAD158b	273.2	0.151	1.059				12.86	2.169	0.362	[4]
	NAC158a	57.34	1.588	0.635	46.98	0.548	0.127	10.75	2.052	0.448	[This work]
	NAC158b	95.33	1.113	0.769				9.48	2.123	0.503	[This work]
200	WOO198	59.2	1.505	0.694	55.8	0.808	0.407	30.1	1.654	0.472	[5]
	NAC200a	53.51	1.599	0.589	30.46	0.531	0.152	9.65	2.107	0.486	[This work]
	NAC200b	84.6	1.113	0.769				9.30	2.123	0.503	[This work]

	Pot. set	V_1 (MeV)	r_1 (fm)	a_1 (fm)	λ [b]	r_c (fm)	Ref.
	α-n	46.71	1.25	0.65	38.0	1.415	[1,10]

[a]Coulomb radius parameter $r_c=1.3$ fm except for the α-n system.
[b]λ factor for an additional spin-orbit term.

In the analysis of the α-α elastic scattering data, the energy dependence in Eq. (1) disappears and the triple integral reduces to a double integral. The Jacobian is now only a function of the mean scattering angle and the differential cross sections are given directly by Eq. (5).

IV. CALCULATIONS

The DWBA theory was employed to interpret the measured energy spectra and angular distributions for the ^{4}He$(\alpha,^3$He$)^5$He(g.s.) reaction. The DWBA calculations were similar to those of Ref. [1], therefore only a brief summary is presented here. Since the ^{5}He final state is unbound, the calculations were performed in zero range with the computer code DWUCK4 [8]. The version of the code used was symmetrized to account for an entrance channel with two identical particles. Nonlocality parameters were set to zero.

Various sets of optical potentials were employed to generate distorted waves for both the entrance and exit channels. Optical-model potentials with six and also with nine parameters were extracted by fitting cross sections calculated with the computer code SNOOPY8 [9] to the measured α-α elastic scattering cross sections obtained from this study. Conventional real and imaginary Woods-Saxon wells comprised the optical potentials of the six-parameter fits, while the real potential component of the nine-parameter fits consisted of the sum of two real Woods-Saxon wells. The latter potential was suggested in Ref. [4] to obtain more flexibility in the shape of the real potential, resulting in an improved fit to their elastic scattering data at 158 MeV. A real Woods-Saxon well with spin-orbit coupling [10], which fits the energy dependence of the p-α phase shifts, was adopted for the α-n interaction. Following Ref. [1], the real central well depth was changed from 45.96 to 46.71 MeV to correctly locate the ^{5}He ground-state peak. With these bound-state parameters of Ref. [1], the energy separation to the first excited $1p_{1/2}$ state in ^{5}He is found to be satisfactorily reproduced. A summary of all the potentials used is presented in Table I.

Center-of-mass double-differential cross sections for the transition to the ^{5}He final state are given by

$$\sigma^{jl}(\epsilon,\theta)=\left(\frac{\mu k}{\pi\hbar^2}\right)\left(\frac{2j+1}{2l+1}\right)D_0^2\sigma^{jl}_{\rm DW}, \tag{6}$$

where μ is the reduced mass, k is the relative wave number, and ϵ is the relative energy of the α-n system; j and l are the total and orbital angular momentum quantum numbers of the transferred nucleon respectively; $\sigma^{jl}_{\rm DW}$ is the DWUCK4 cross section and D_0^2 is a strength factor to correct for finite-range effects. Contributions from both the $1p_{3/2}$ and $1p_{1/2}$ states in ^{5}He were calculated for values of ϵ ranging from 0 to 5 MeV and added incoherently to obtain the double-differential cross sections, which were subsequently integrated according to Eq. (3) to obtain the energy-integrated differential cross sections. At the energies of the present work the $1p_{1/2}$ state contributes of the order of 1% to the cross section, which is in agreement with findings of Warner *et al.* [1].

Theoretical values for the D_0^2 strengths were obtained from ratios of the calculated total cross section given by corresponding finite-range and zero-range DWBA calculations, assuming the ^{5}He final state to be bound by 0.1 MeV. The computer code DWUCK5 [11], which was also symmetrized for an entrance channel with two identical particles, was used for these finite-range calculations.

V. RESULTS AND DISCUSSION

Before presenting the DWBA analysis of the transfer reaction data, the optical potentials extracted from elastic scat-

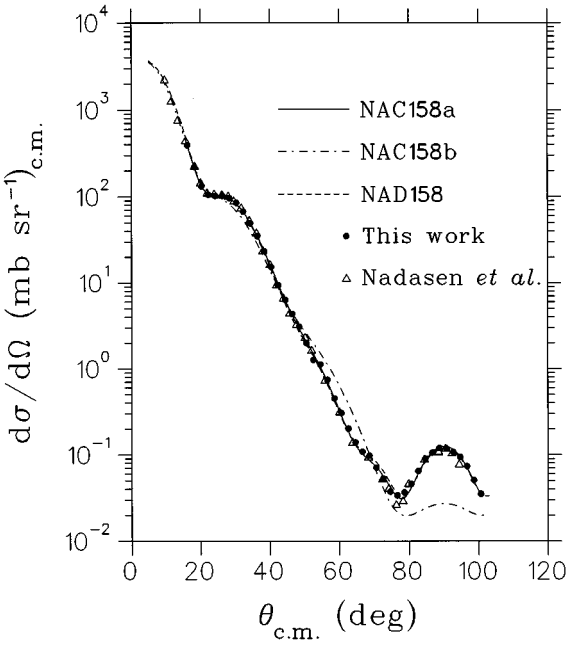

FIG. 1. Elastic scattering cross sections for $\alpha+{}^4$He at $E_\alpha=158$ MeV. The measurements obtained in this work are compared with measurements by Nadasen *et al.* [4]. The curves are optical-model fits, the parameters of which are presented in Table I.

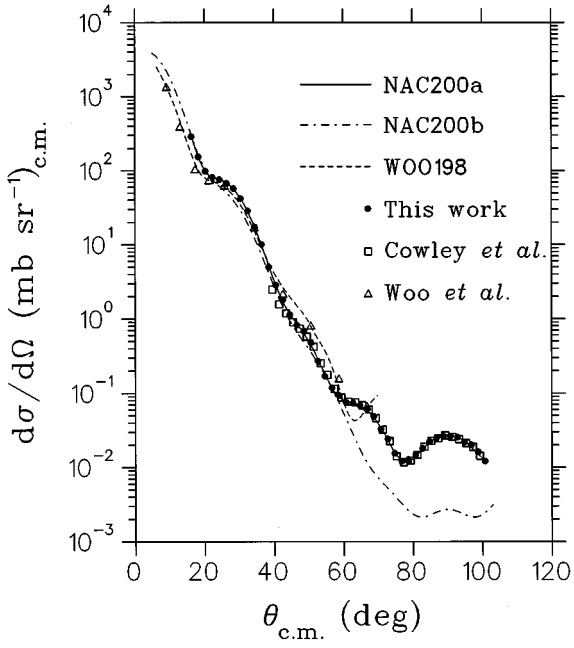

FIG. 2. Elastic scattering cross sections for $\alpha+{}^4$He at $E_\alpha=200$ MeV. The measurements obtained in this work are compared with measurements by Woo *et al.* [5] and our earlier work [6]. The curves are optical-model fits, the parameters of which are presented in Table I.

tering data, which were needed for the DWBA calculations, are discussed.

A. Elastic scattering and optical potentials

The α-α elastic scattering cross sections measured at an incident energy of 158 MeV are shown in Fig. 1, along with the measured data of Nadasen *et al.* [4]. Good overall agreement is evident and the present results therefore confirm the previous data.

In Fig. 2 the measurements of the elastic angular distribution at an incident energy of 200 MeV are compared with our previous measurements at 197 MeV [6], as well as with the measurements of Woo *et al.* at 198.4 MeV [5]. In Ref. [6] the symmetry of the angular distribution around 90° (c.m.) was exploited by presenting measurements performed in the backward c.m. hemisphere at forward angles. The agreement of our previous results with the results of the present study is satisfactory. However, Ref. [6] presents only a partial data set since the experimental setup used did not allow cross sections to be measured at angles smaller than ~40° (c.m.). The measurements of Woo *et al.*, on the other hand, do not extend to the larger angles, covering only the angular region from ~10°–65° (c.m.). At these angles the present measurements display a somewhat steeper slope and the overall agreement is clearly not satisfactory.

Optical-model fits for potentials extracted in this as well as previous studies (Nadasen *et al.* [4] and Woo *et al.* [5]) are shown in Figs. 1 and 2. The nine-parameter optical potentials (NAC158a and NAC200a—see Table I) describe the measured elastic scattering data of the present study very well, producing optical-model fits with χ^2/N values of 1.5 and 0.6 at 158 and 200 MeV, respectively, assuming a 5% systematic experimental uncertainty. The 158 MeV potential sets NAC158a (this study) and NAD158a (Ref. [4]) are very similar, which is to be expected as they were extracted from measured data sets which are in good agreement. At 200 MeV, however, the agreement with the potential set of Ref. [5] is poor. This could be largely due to the absence of measurements at larger angles in the data set from which the last-mentioned potential set (WOO198—see Table I) was extracted.

At both incident energies of this study, six-parameter optical-model fits which describe the measured α-α elastic angular distributions to the same accuracy as the nine-parameter sets could not be found. The sensitivity to the specific choice of parameters of conventional Woods-Saxon potentials near 90° (c.m.) is well known [12]. We therefore based our search for six-parameter potentials on the requirements that the average slope from forward scattering angles down to about 60° (c.m.) should be reproduced, that the magnitudes of the real and imaginary volume integrals of the corresponding nine-parameter potentials should be retained, that the geometrical parameters should be physically realistic and that the predicted total cross sections should be in agreement with calculations utilizing the nine-parameter potentials. Differences encountered in the angular region around 90°(c.m.) were ignored. The resulting potentials (NAC158b and NAC200b) are presented in Table I and the corresponding predictions for the α-α elastic scattering cross sections are also shown in Figs. 1 and 2.

The energy dependence of the real and imaginary potential volume integrals was investigated by comparing our results at 200 MeV with the data analyzed by means of two-component real potentials by Nadasen *et al.* [4] at incident energies of 53.4, 77.6, 99.6, 119.9, 140, and 158.2 MeV (see Fig. 3). Values obtained by Woo *et al.* [5] for both the real

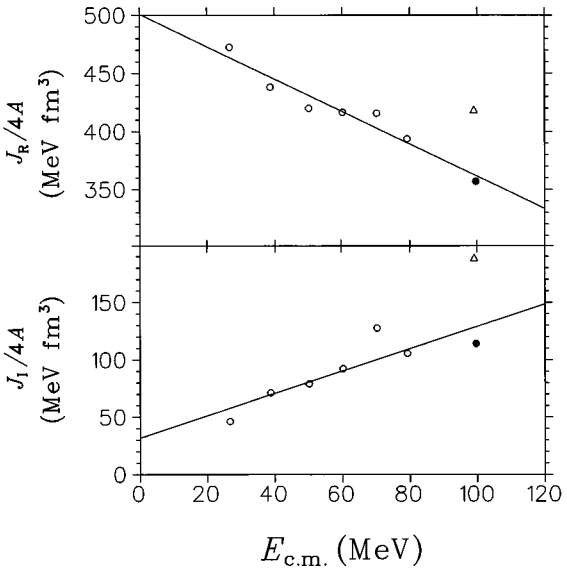

FIG. 3. Energy dependence of the real and imaginary volume integrals from optical-model analyses of α-α elastic scattering data as displayed by the straight lines (see text). The open circles are the results published by Nadasen *et al.* [4], the closed circles are the results of this study at 200 MeV, and the open triangles are the results of Woo *et al.* [5].

and imaginary volume integrals are also shown in Fig. 3. Despite the scatter, it seems as if the values of Ref. [5] are anomalously high for both $J_R/4A$ and $J_I/4A$. In fact, based on their results, these authors questioned the energy dependence of the real volume integral claimed in Ref. [4]. Our results seem to support the energy dependences found by Nadasen *et al.* for both the real and imaginary volume integrals. If the results of Woo *et al.* at 198 MeV are excluded, linear least-squares fits yield energy coefficients (slopes) of -1.4 ± 0.16 fm^3 for $J_R/4A$ and 1.0 ± 0.25 fm^3 for $J_I/4A$, which are found to be in excellent agreement with the respective values of -1.3 ± 0.3 fm^3 and 1.0 ± 0.3 fm^3 of Ref. [4].

B. Single-nucleon transfer to the ^{5}He ground state

Measured ^{3}He energy spectra and results from corresponding DWBA calculations in the region of the ^{5}He(g.s.) peak are shown in Figs. 4 and 5 for incident energies of 158 and 200 MeV, respectively. Calculations obtained from the nine-parameter optical-model fits of this study (NAC158a and NAC200a—see Table I) are shown, but the six-parameter potentials yield similar results. Each calculated cross section was folded with an experimental uncertainty, the width of which was taken to be equal to the measured width of the corresponding α-α elastic peak. By normalizing the calculations arbitrarily to the measured ^{5}He(g.s.) peaks, generally good agreement is obtained. Some deviations are found at forward angles towards lower ^{3}He energies (for values of $\epsilon \gtrsim 2.5$ MeV), but these become less pronounced towards larger angles.

The good qualitative agreement between DWBA calculations and the experimental data in the region of the ^{5}He(g.s.) peak provides confidence in the procedure of extracting cross sections by integrating over ϵ in the region $0 \leqslant \epsilon \leqslant 5$ MeV. It therefore also seems reasonable to assume that mechanisms not treated by the DWBA, such as knockout and multistep processes, do not contribute significantly in this energy region.

The angular distributions of the energy-integrated differential cross sections are shown in Figs. 6 and 7 for incident energies of 158 and 200 MeV, respectively. The experimental cross sections are compared with DWBA calculations performed with the potentials listed in Table I.

At 158 MeV, zero-range DWBA calculations with the nine-parameter optical potential set extracted in this study (NAC158a) yield a prediction that deviates significantly in shape from the measurements (see Fig. 6). This is in contrast to the results at 118 MeV [1], where a sharp minimum at 90° (c.m.) characterized the calculated angular distribution,

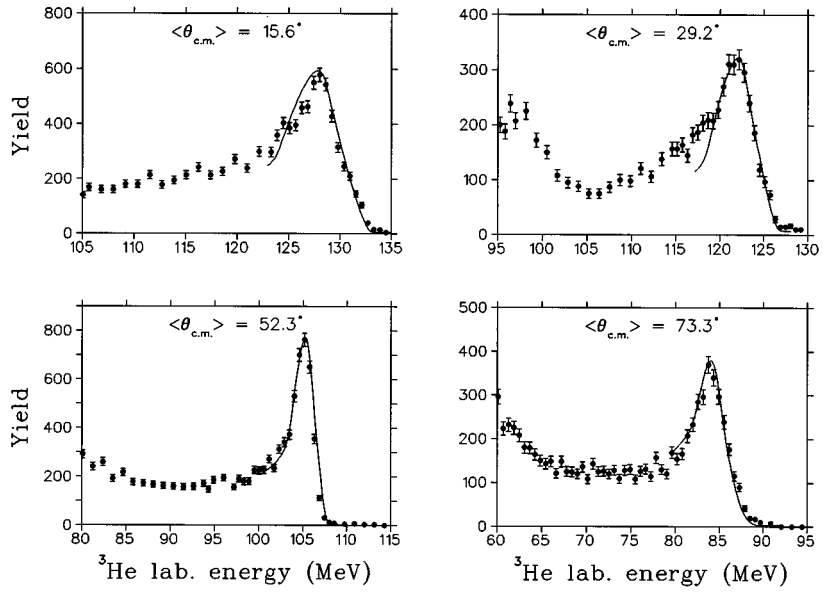

FIG. 4. Laboratory energy spectra of ^{3}He from the ^{4}He(α,^{3}He)^{5}He reaction at $E_\alpha = 158$ MeV. Selected mean c.m. scattering angles $\langle\theta_{\rm c.m.}\rangle$ correspond to laboratory angles $\theta_{\rm lab}$ as follows: $\theta_{\rm lab}(\langle\theta_{\rm c.m.}\rangle)$; 8.0°(15.6°); 15.0°(29.2°); 27.0°(52.3°); 38.0°(73.3°). The curves are DWBA predictions for $0 \leqslant \epsilon \leqslant 5$ MeV (see text), normalized arbitrarily to the measured ^{5}He ground-state peaks.

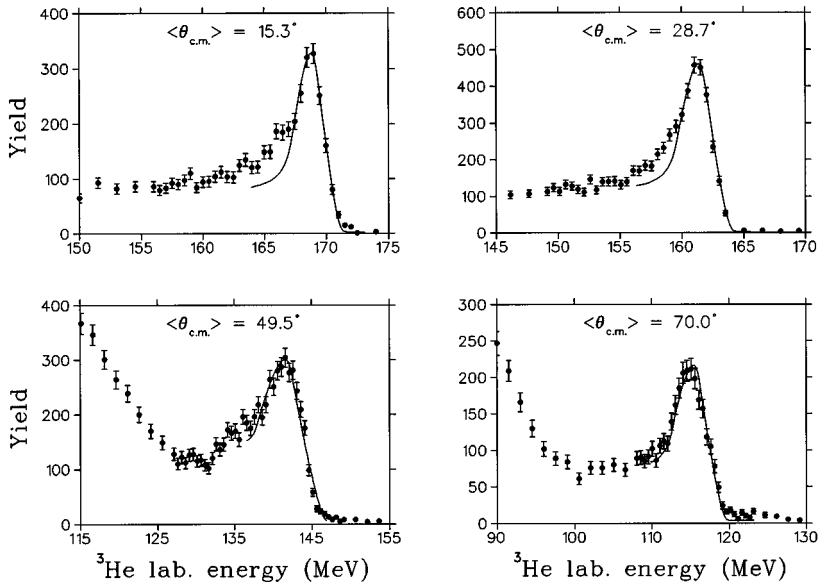

FIG. 5. Energy spectra of ^{3}He from the ^{4}He(α,^{3}He)^{5}He reaction at $E_\alpha = 200$ MeV. Selected mean c.m. scattering angles $\langle\theta_{\text{c.m.}}\rangle$ correspond to laboratory angles θ_{lab} as follows: $\theta_{\text{lab}}(\langle\theta_{\text{c.m.}}\rangle)$; 8.0°(15.6°); 15.0°(29.2°); 26.0°(52.3°); 37.0°(73.3°). For further details, see caption to Fig. 4.

and the slope (on a logarithmic scale), although being somewhat steeper than that of the measurements, nevertheless reproduced the shape of the measured cross sections reasonably well. In the present study at 158 MeV, however, the DWBA calculations with the nine-parameter potential set produce a broad global minimum, extending from about 70° to 110° (c.m.), while the average slope between about 30° and 70° (c.m.) is significantly steeper than revealed by the measurements. To investigate this strange behavior, we also performed calculations with the nine-parameter optical potentials of Ref. [1] (WAR118) at both 118 and 158 MeV. While the 118 MeV results of Ref. [1] could be reproduced exactly, the above-mentioned qualitative discrepancy at 158 MeV (see Fig. 6) remains. It is interesting to note that different nine-parameter optical potentials yield similar anomalous results. One possible explanation for this is that representing the real component as the sum of two attractive real Woods-Saxon wells, although reproducing elastic α-α scattering data very well, may lack a sound physical basis. Consequently, these potentials may yield an unphysical description of the ^{3}He and ^{5}He distorted waves in the exit channel. Absolute normalization of the calculated DWBA cross sections was achieved by using theoretical D_0^2 strengths obtained in the manner described before, the values of which are presented in Table II.

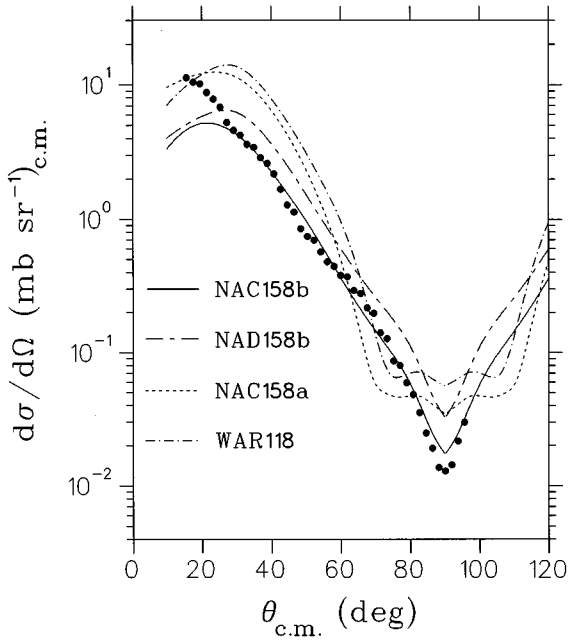

FIG. 6. Center-of-mass differential cross sections for the ^{4}He(α,^{3}He)^{5}He(g.s.) reaction at $E_\alpha = 158$ MeV. Both measured and theoretical predictions are integrated over the ^{3}He energy region corresponding to $0 \leq \epsilon \leq 5$ MeV for central rays. The optical-model parameters used in the DWBA calculations (shown as curves) are presented in Table I. The six- and nine-parameter potential sets of this study at 158 MeV are denoted by NAC158b and NAC158a, respectively. NAD158b is the six-parameter potential set of Ref. [4] and WAR118 the nine-parameter potential set of Ref. [1]. Statistical error bars are shown only where these exceed the symbol size. Normalizations for the results of all potential sets are as given by the theoretical values of D_0^2, except for the set NAC158b, the results of which are normalized to the experimental data (see Table II).

The DWBA calculations for an incident energy of 158 MeV utilizing the six-parameter optical potentials extracted in this study (NAC158b) predict theoretical cross sections which are in much better agreement with the experimental data (see Fig. 6). Normalization to the measured cross sections yields an experimental D_0^2 strength of 1.7×10^4 MeV^2 fm^3, which is a factor of $\sim$2.6 smaller than the corresponding theoretical value (see Table II). An additional calculation shown in Fig. 6 was obtained by using the six-parameter optical potential set of Ref. [4] (NAD158b), which has an unphysically narrow and very strongly attractive real Woods-Saxon well. Although predicting a somewhat higher theoretical D_0^2 strength, satisfactory agreement in shape is found with the previous six-parameter calculation and with the measurements. This result is significant, considering the very different characteristics of the two six-parameter optical potential sets (NAC158b and NAD158b) used.

The measured cross sections at an incident energy of 200

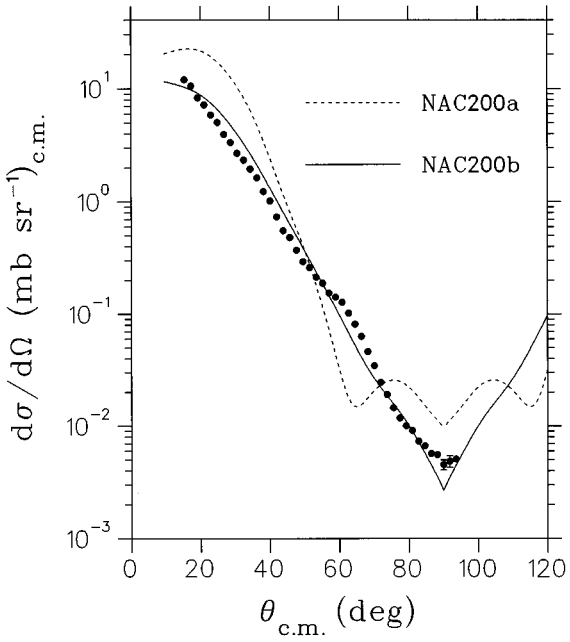

FIG. 7. Center-of-mass differential cross sections for the ^{4}He(α,^{3}He)^{5}He(g.s.) reaction at $E_\alpha = 200$ MeV. The six- and nine-parameter potential sets of this study at 200 MeV are denoted by NAC200b and NAC200a, respectively. The results for the potential set NAC200a are normalized by the theoretical value of D_0^2, while the results for the set NAC200b are normalized to the experimental data (see Table II). For more details, see caption to Fig. 6.

MeV, together with the corresponding DWBA calculations utilizing both the six- and nine-parameter optical potentials of this study at 200 MeV (NAC200b and NAC200a—see Table I), are shown in Fig. 7. Similarity to the corresponding results at 158 MeV is evident. While calculations performed with the six-parameter potential set predict the measurements well, calculations utilizing the nine-parameter potential set seem to be inappropriate. An experimental D_0^2 strength of 2.9×10^4 MeV^2 fm^3 is found by normalizing the six-parameter potential (NAC200b) calculation to the measured data. This value is a factor of $\sim$1.7 smaller than the theoretical prediction.

The measured angular distributions at 158 and 200 MeV and of Ref. [1] at 118 MeV are characterized by a predominantly exponential form. All three sets of measurements are reasonably well reproduced in the forward c.m. hemisphere by the phenomenological expression

$$\left(\frac{d\sigma}{d\Omega}\right)_{\text{c.m.}} = a\exp[-(b+c\langle E_\alpha\rangle_{\text{c.m.}})\theta], \tag{7}$$

where $\langle E_\alpha\rangle_{\text{c.m.}}$ is the incident c.m. energy at the mean α-n relative energy $\langle\epsilon\rangle$, θ is the c.m. scattering angle, and the coefficients are $a=68.1$, $b=2.05\times10^{-2}$, and $c=1.19\times10^{-3}$. The single normalization factor, a, indicates that the three sets of measurements converge to values of similar magnitude at small angles. The slopes of the angular distributions (on a logarithmic scale) are, however, found to reveal an energy dependence, characterized by increasing steepness with increasing incident energy.

TABLE II. Experimental and theoretical predictions of D_0^2 for the reaction ^{4}He(α,^{3}He)^{5}He (g.s.).

E_α (MeV)	Pot. set	$D_0^2/10^4$ (MeV^2 fm^3) Theoretical	Experimental
158	WAR118	4.24	
	NAD158b	5.53	
	NAC158a	4.57	
	NAC158b	4.44	1.7
200	NAC200a	5.05	
	NAC200b	5.00	2.9

VI. SUMMARY AND CONCLUSIONS

The present measurements are found to be in agreement with previous results of α-α elastic scattering at 158 MeV, while significant differences at 200 MeV are found with respect to one of the earlier measurements. Real and imaginary volume integrals of the optical potentials extracted in this study support the energy dependences found in an earlier study at 158 MeV, in contrast to a previous result at 200 MeV. This is a strong indication that the present elastic scattering cross-section values at 200 MeV are also reliable.

This study has shown that the shapes of the ^{3}He energy spectra in the region of the ^{5}He ground-state peak are well reproduced by appropriate DWBA calculations at incident energies of 158 and 200 MeV, which is consistent with previous results at 118 MeV. However, nine-parameter optical potentials comprising two attractive real Woods-Saxon wells, which describe elastic scattering accurately, are found to yield unsatisfactory results for the angular distributions of the ^{4}He(α,^{3}He)^{5}He(g.s.) reaction at both these incident energies. This problem could be resolved to a large extent by utilizing six-parameter optical potentials. The ratios of finite-range to zero-range calculations yield theoretical D_0^2 strengths that generally overpredict the energy-integrated differential cross sections, by factors of $\sim$2.6 and $\sim$1.7 for these potential sets at 158 and 200 MeV, respectively. This is consistent with the previous study at 118 MeV which reported an overprediction by a factor of $\sim$2 at forward angles. Also, the theoretical D_0^2 strengths of this study are in agreement with the value found at a lower incident energy.

Consequently, the theoretical overprediction of the ^{4}He(α,^{3}He)^{5}He(g.s.) cross section persists at higher incident energies. At these energies the DWBA should be even more reliable than at the lower incident energy investigated previously. Clearly, the reason for the observed discrepancy needs to be investigated further.

ACKNOWLEDGMENTS

The authors wish to thank Professor P. D. Kunz for making symmetrized versions of the codes DWUCK4 and DWUCK5 available to this study, and also for valuable information and advice on the relevant DWBA calculations. We are grateful to Dr. A. H. Botha and his personnel for providing high quality alpha beams.

[1] R. E. Warner, J. M. Fetter, R. A. Swartz, A. Okihana, T. Konishi, T. Yoshimura, P. D. Kunz, M. Fujiwara, K. Fukunaga, S. Kakigi, T. Hayashi, J. Kasagi, and N. Koori, Phys. Rev. C **49**, 1534 (1994).

[2] F. Ajzenberg-Selove, Nucl. Phys. **A490**, 1 (1988).

[3] N. Austern, R. M. Drisko, E. C. Halbert, and G. R. Satchler, Phys. Rev. **133**, B3 (1964).

[4] A. Nadasen, P. G. Roos, B. G. Glagola, G. J. Mathews, V. E. Viola, Jr., H. G. Pugh, and P. Frisbee, Phys. Rev. C **18**, 2792 (1978).

[5] L. W. Woo, K. Kwiatkowski, S. H. Zhou, and V. E. Viola, Phys. Rev. C **32**, 706 (1985).

[6] A. A. Cowley, G. F. Steyn, S. V. Förtsch, J. J. Lawrie, J. V. Pilcher, F. D. Smit, and D. M. Whittal, Phys. Rev. C **50**, 2449 (1994).

[7] J. V. Pilcher, A. A. Cowley, D. M. Whittal, and J. J. Lawrie, Phys. Rev. C **40**, 1937 (1989).

[8] P. D. Kunz, and E. Rost, in *Computational Nuclear Physics 2 – Nuclear Reactions*, edited by K. Langanke, J. A. Maruhn, and S. E. Koonin (Springer-Verlag, New York, 1993), p. 88.

[9] P. Schwandt, ''SNOOPY8 – Optical Potential Code for Elastic Scattering Analysis,'' IUCF Report No. 82-3 (1982).

[10] P. D. Kunz, A. Saha, and H. T. Fortune, Phys. Rev. Lett. **43**, 341 (1979).

[11] P. D. Kunz, computer code DWUCK5 (unpublished).

[12] N. Rowley, H. Doubre, and C. Marty, Phys. Lett. **69B**, 147 (1977).